RSC Advances




ROYAL SOCIETY OF CHEMISTRY

www.rsc.org/advances

Journal Name

ARTICLE

# Liquid Crystal Graphene Oxide with different layers: Fabrication, Characterization and Applications

Received 00th January 20xx,
Accepted 00th January 20xx

DOI: 10.1039/x0xx00000x

www.rsc.org/

Jianmin Zhang, Yumei Ren, Tao Xu, Hongxia Yang and Qun Xu*

A series of graphene oxide (GO) nanosheets with monolayer, bilayer and multilayer were prepared merely via a simple centrifugation method. It is noticeable to address that the as-prepared bilayer and multilayer GO nanosheets aqueous dispersions exhibit the liquid crystals (LCs) behavior. Not only the liquid- but also the solid-state of the obtained GO presented prominent functional LCs behavior. Then GO films can be fabricated via simple drop-casting of concentrated GO (cGO) aqueous dispersions that retain the radial schlieren texture and show excellent electrical conductivities of 12 S/cm after chemical reduction. Thus it can be expected utilizing the coating property of GO aqueous dispersions as well as the prominent birefringent linear features of the cGO films, will have great potential to prepare functional anti-counterfeiting components and energy materials.

## Introduction

Graphene oxide liquid crystals (GO LCs) is of potential technological interest because the self-assembly of GO sheets produced by the liquid-crystalline process can exhibit multifunctional attributes such as high mechanical strength, excellent flexibility, and an important precursor of ordered graphene building blocks.[1,2] Compared to other approaches developed to align GO sheets, the liquid-crystal route is particularly attractive to achieve self-assembly with graphene-based materials in the form of fibers and films.[3,4,7,8] The liquid-crystalline behavior of monolayer GO sheets has been reported.[1-8] Recently, even liquid-crystalline behavior of graphite oxide sheets have also been confirmed. [9] Further, it is interesting to know how about the pure bilayer or multilayer of GO sheets, and is there liquid-crystalline behavior for them? In earlier work, size-selective fractionation of GO sheets has been reported. Sun et al. developed a density gradient ultracentrifugation method for the fractionation of GO sheets.[10,11] Shi et al. invented a rapid and simple size separation method based on the pH-dependent amphiphilicity of GO sheets.[12] However, thickness-selective fractionation of GO sheets has never been reported.

Here, we reported the separation of GO sheets with different layers by simple centrifugation, and then multilayer, bilayer and monolayer GO sheets are obtained. Our experimental results indicate that not only the monolayer but also the bilayer or multilayer GO sheets both can form a LC in their aqueous dispersions. More importantly, the GO films that were prepared with GO LCs can retain the radial schlieren texture. Further, graphene films can be obtained by simple drop-casting of GO dispersions combined with chemical reductions, which possess fine flexibility and high electrical conductivity. Moreover it can be tested that the macroscopic solid materials can be well used in optical fields such as anti-counterfeiting material.

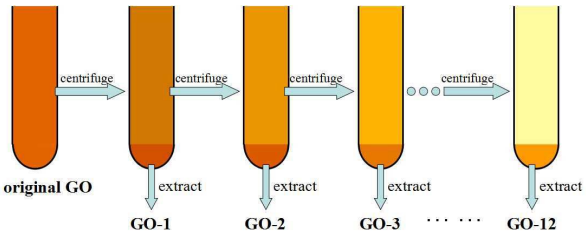


Scheme 1 Schematic protocol to separate GO sheets with different layers.

## Results and discussion

Scheme 1 shows the fabrication process of GO sheets with the varying layers via a series of centrifugation. GO was synthesized from graphite powder by a modified Hummers method.[13,14] GO sheets with different layers were obtained by simple centrifugation (see ESI†), which could be confirmed by atomic force microscopy (AFM) measurements. Fig. 1a, 1b and 1c show the representative AFM images of the GO sheets obtained from three different cycles. It can be clearly observed that the thickness of the GO sheets decreases with the increasing of the cycle times. According to the AFM measurements (Fig. S3, S4 and S5, ESI†), the thickness and width distribution of each sample can be obtained. Typically, for GO-1, GO-6 and GO-12, their thickness is about 2 nm, 1.6 nm and 1 nm, respectively (Fig. 1d, 1e and 1f). According to the uniform thickness in same sample and the linear decrease in the thickness from GO-1 to GO-12, we infer the three samples have different

[a] College of Materials Science and Engineering, Zhengzhou University, Zhengzhou 450052, China. E-mail: qunxu@zzu.edu.cn; Fax: +86 371 67767827; Tel: +86 371 67767827

† Footnotes relating to the title and/or authors should appear here.
Electronic Supplementary Information (ESI) available: [details of any supplementary information available should be included here]. See DOI: 10.1039/x0xx00000x

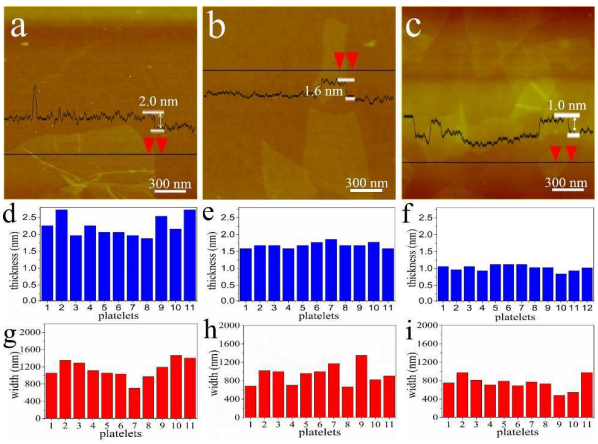


Fig. 2 Representative AFM images of the GO sheets deposited on silicon wafer from GO-1, GO-6, GO-12 aqueous solution (a, b, c) and their corresponding thickness distributions (d, e, f) and width distributions (g, h, i).

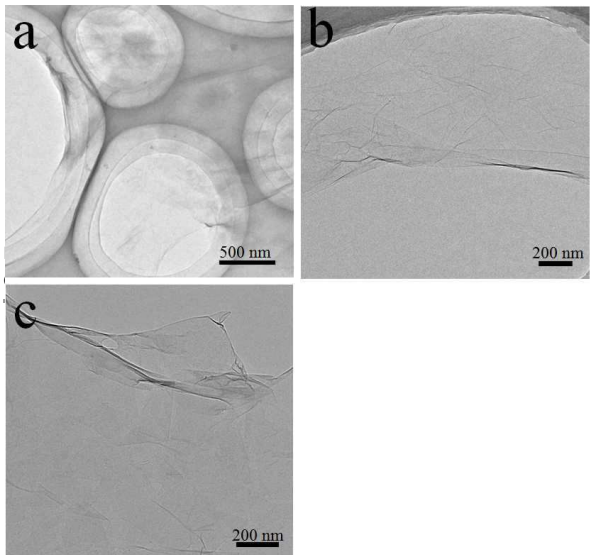


Fig. 1 TEM images of GO-1 (a), GO-6 (b), GO-12 (c). The samples were deposited on copper screens (325 mesh)

sheet layers and they are multilayer, bilayer and monolayer for GO-1, GO-6 and GO-12, respectively.[15] The thickness values of multilayer GO sheets are much less than three times of the values of monolayer GO sheets, we think the multilayer GO sheets compare with the monolayer have less oxygen-containing functional groups , result in that the experimental thickness is lower than the theoretical thickness.[16] Moreover, their lateral width are also reductive and average lateral width are 1148 nm, 933 nm and 746 nm (Fig. 1g, 1h and 1i). For GO-1, GO-6 and GO-12, average values for W/T of individual sheets are $5.13\times10^{2}$, $5.5\times10^{2}$ and $7.34\times10^{2}$, respectively, indicating the average W/T values are decreasing with the increasing of the cycle times.

The decreasing trend of thickness is also confirmed by transmission electron microscopy (TEM), which is shown in Fig. 2. And the results illustrate that the thickness of GO-6 and GO-12 is

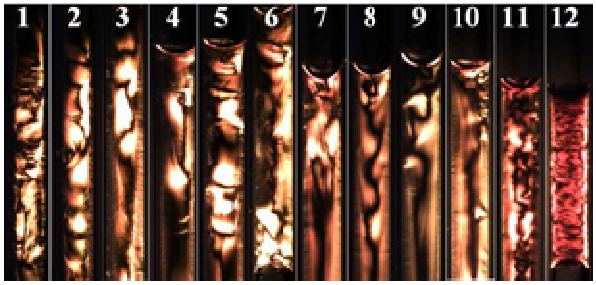


Fig. 3 POM images of GO aqueous dispersions from cGO-1 to cGO-12 in capillaries observed between crossed polarizers.

thinner than that of GO-1, which is in good agreement with the results of AFM.

In a previous study, graphene oxide has been proven to be a highly heterogeneous material that consists of poorly oxidized graphene sheets and highly oxidized graphene debris.[17] The poorly oxidized graphene sheets were thicker and bigger than highly oxidized graphene debris that means may preferentially settling to the bottom of centrifugal tube by centrifugal forces. To test this hypothesis and further explore the influencing factors of exfoliation, Raman spectra and X-ray-photoelectron-spectroscopy (XPS) were used to characterize the obtained GO sheets. Fig. S6 (ESI†) shows the high frequency Raman spectra of GO sheets with different layers. Raman spectra of the samples displays two characteristic peaks at 1356 and 1595 $cm^{-1}$, which represent the D-band (C–C, the vibrations of $sp^3$ carbon atoms of defects and disorder) and G-band (C=C, the vibration of $sp^2$ carbon atoms in a graphitic 2D hexagonal Lattice), respectively.[18] In general, the degree of graphitization is an indicator of the graphene sheets' disorder level and is characterized by the intensity ratio of the D and G bands (R = ID/IG). The ID/IG ratio of GO-1, GO-6 and GO-12 is 0.84, 0.89 and 0.94, respectively. The increasing ID/IG ratio indicates that the graphitic 2D hexagonal lattice has been severely disturbed, which weakens the van-der-Waals forces between GO layers.

As known to us, electrostatic repulsion, due to the presence of electronegative oxygen-containing functional groups, also has an influence on van-der-Waals forces between GO layers.[19] Hence, the oxygen content may be a major factor to affect this interactions. XPS measurement was always carried out to identify the chemical species, which can be used as a direct evidence to measure the oxygen content.[20,21] The results from the XPS analysis are shown in Fig. S7 (ESI†). And the C1s spectra are compared among different cycles of GO samples. As can be seen from the C1s XPS spectrum of GO, it clearly indicates a considerable degree of oxidation with four different components corresponding to the following functional groups: sp2-hybridized C-C/C=C in aromatic ring (284.6 eV), C-O (286.7 eV), C=O (287.7 eV), and C(O)OH (290 eV). The atomic ratios of C1s /O1s decrease from 2.793 to 2.660 for GO-1 and GO-2. So the oxygen amount increases with the increasing of cycle times, implying that it is closely related with the exfoliation of GO. The more oxygen content means more negative charges, which results in stronger repulsive forces between GO sheets, making GO sheets more easily exfoliate.4,6 From the results of Raman and XPS, it can be concluded that van-der-Waals forces between GO sheets are

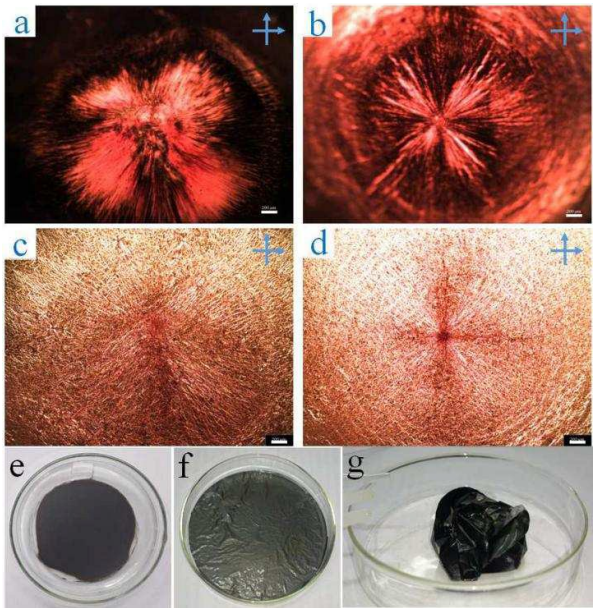


Fig. 4 POM images of liquid- and solid-state of cGO aqueous dispersions for cGO-1 (a, c), cGO-2 (b, d) on microslides observed between crossed polarizers. The scale bar represents 200 μm. Optical photographs of cGO-1 films (e) before and (f) after chemical reduction, the flexible rGO-1 film (g).

affected by the defects of 2D hexagonal lattice and electronegative oxygen-containing functional groups. The decrease of the van-der-Waals forces between GO sheets owning to the enhancive defects and/or the increased oxygen content can contribute to the exfoliation of GO sheets.

As far as we know, a high concentration of GO aqueous dispersions is a prerequisite to form a lyotropic LC. In this work, twelve groups of concentrated GO (cGO) aqueous dispersions were obtained via centrifuging. The fm (mass fraction) of cGO aqueous dispersions are 2.5 × 10-2, 1.7× 10-2, 1.2 × 10-2, 1.0 × 10-2, 0.8 × 10-2, 0.8× 10-2, 0.9× 10-2 for cGO-1, cGO-2, cGO-4, cGO-6, cGO-8,

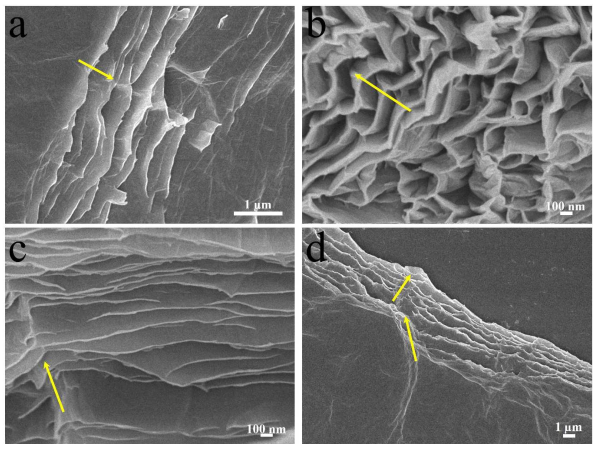


Fig. 5 SEM images of fracture morphology of the freeze-dried solid of cGO-1 (a), cGO-4 (b), cGO-8 (c), cGO-12 (d); and the arrows indicate the alignment directions of the wrinkles.

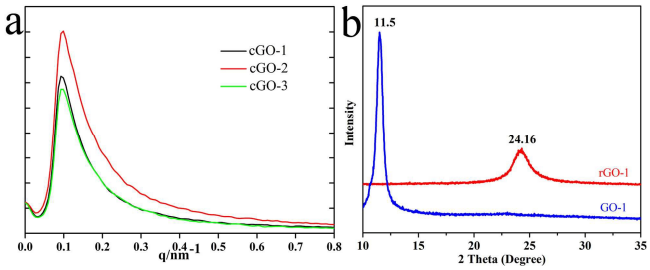


Fig. 6 SAXS spectra of films for cGO-1, cGO-2 and cGO-3, the spectra depict the scattering intensity as a function of scattering vector q (q = (4π sin θ)/λ, where 2θ is the scattering angle) (a), XRD patterns of cGO-1and rGO-1 films (b).

cGO-11 and cGO-12, respectively. And the fm are falling with the increasing of the cycle times except cGO-12 (see ESI†). Fig. 3 shows the prominent optical birefringence of the twelve concentrated GO (cGO) in capillaries between two crossed polarizers by polarized-light optical microscopy (POM), which confirms the formation of the lyotropic LC. Compare the Fig. 1 and Fig. 3, we can see that cGO-12 with the thickness of 1.0 nm presents the typical optical birefringence, which is in agreement with the previous reports. Moreover, we find out that both GO-6 and GO-1 with bilayer and multilayer also have the LC behavior. However, the optical birefringence of the twelve capillaries has no distinct difference along with the decreasing cGO concentration except cGO-12, which is due to an increased concentration of cGO-12 resulted in a more colorful optical birefringence. Using the frame of Onsager's theory, the concentrations for phase transition from the isotropic phase to the nematic phase is approximately linearly dependent on thickness/width ($f_m \approx kT/W$, k is a constant).[2,22] It means that a higher value of W/T indicates a lower point of transitional concentration to an ordered mesophase, and the increasing value of W/T for cGO-1, cGO-6 and cGO-12 are $5.13\times10^2$, $5.5\times10^2$ and $7.34\times10^2$ from the data of Fig.1 suggest a reductive trend of concentration, this is in accordance with our actual measured concentration changes. Moreover, the optical birefringence were more and more colourful from cGO-1 to cGO-12 when cGO-1 and cGO-6 were diluted to the same concentration of cGO-12 (Fig. S8). This also conforms to the frame of Onsager's theory.

To ascertain liquid-crystalline phases of the cGO samples, they were observed by POM on glass slide. The liquid-crystalline schlieren texture in Fig. 4(a, b) is very similar to typical nematic samples. Meanwhile, the corresponding solid-state of cGO dispersions also demonstrates radial schlieren textures (Fig. 4c, d). For investigating the radial schlieren textures of organized solids, scanning electron microscopy (SEM) images were collected. As shown in Fig. 5, fracture morphology of the freeze-dried solid derived from the cGO dispersions displays orientational arrangement. In the solid films, ordered alignments of wrinkles perpendicular to the sheet planes are clearly observed, with orientational directions as marked by arrows. These radial schlieren textures appear at solid-state of the cGO dispersions may attribute to arrangement of the GO wrinkles.[23]

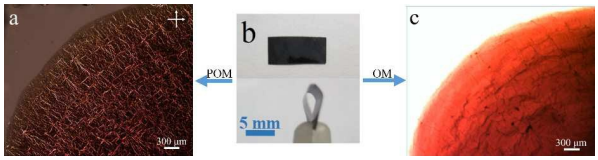


Fig. 7 Optical photographs of cGO films (b) as anti-counterfeiting materials by polarizing microscope (POM) (a), by optical microscope (OM) (c).

Figure 6a shows the SAXS results of the corresponding solid-state of cGO dispersions for cGO-1, cGO-2 and cGO-3. Scattering peak at q=0.09 $nm^{-1}$ arising from the diffraction of the ordered flakes, reflecting the uniformity of the spacing between the flakes, indicating the three different cycle samples have a same oriented alignment of sheets, which is also in agreement with the results of the optical birefringence of the twelve concentrated GO (cGO) in capillaries in figure 3.[24]

Free-standing GO film was fabricated via simple drop-casting of cGO aqueous dispersions and it is shown in Fig. 4e. It is well known that the insulating GO can be easily converted to conductive graphene by either chemical or thermal reduction.[25-27] Herein, the rGO-1 flexible films can be prepared by chemical reduction of cGO-1 films using hydroiodic acid aqueous solution as the reducing reagent.[28,29] After chemical reduction, rGO-1 flexible film has a metallic luster (Fig. 4f, g). In the chemical reduction process, there are two chemical structural evolutions: the elimination of pendant oxygen-containing functional groups such as hydroxyl and epoxy groups and the restoration of conjugated carbon net, which are proven by the detailed characterizations of XPS, Raman and X-ray diffraction (XRD). Fig. S7a and S9 (ESI†) show the XPS survey spectra of cGO-1 films and rGO-1 flexible films, and the atomic ratios of C1s/O1s increase from 2.79 to 8.75. This verifies that the removal of oxygen functional groups maybe accompany the recovery of conjugated network. The 2D peak (2680 $cm^{-1}$) in the Raman spectrum (Fig. S10, ESI†) is obviously increased after reduction, also strongly suggesting the restoration of $sp^2$ carbon in rGO films.[5,29,30] The increase in the ratio of I(D)/I(G) (1.30) for rGO-1 compared to cGO (0.84) suggests an increase of disorder in microstructures of the reduced GO thanks to the presence of unrepaired defects that remained after the removal of oxygen moieties. XRD spectrum shows that the interlayer distance of the rGO-1 film (Fig. 6b) decreases to 3.68 Å (2θ = 24.16˚) from 7.69 Å (2θ = 11.5˚) for the cGO-1 film, which is attributed to the elimination of the oxygen-containing groups on the graphene sheets.

Mechanical tensile measurements demonstrate that both GO films and rGO films exhibit typical plastic deformation under tensile loading at room temperature (Fig. S11, ESI†). The initiating regions in tensile curves are possibly due to the stretching of the wrinkled GO and rGO sheets. The Young's moduli of GO films and rGO films are 96 MPa and 46 MPa individually. Upon further straining, GO films and rGO films show typical fracture strengths of 1.9 and 3.9 MPa, and ultimate elongations of 2.6% and 3.9%, respectively. This enhanced strength could be ascribed to the stronger interactions between graphene sheets coming from the more compact stacking of the graphene films.[29,31] Moreover, rGO films show excellent electrical conductivities of 12 S/cm, which is higher than that in previous reports thanks to the fine alignment of graphene sheets resulting from the self-assembly of GO LCs.[32-35] Utilizing the prominent birefringent linear features of cGO films, we tried to employ them to optical anti-counterfeit technology. As shown in Figure 7, the cGO film (Fig. 7b) shows the prominent emergence of microscopic birefringence between two crossed polarizers (Fig. 7a), while no obvious patterns can be observed from the cGO film in ordinary optical microscope (OM) (Fig. 7c). The appearance and disappearance of the patterns upon POM and OM are completely reversible due to this simple physical optical transition.

## Conclusions

In summary, GO LCs with different sheet layers were successfully prepared, and GO films fabricated via simple drop-casting of cGO aqueous dispersions can show excellent electrical conductivities of 12 S/cm after chemical reduction. Besides, their extraordinary birefringent linear features can be used to the functional anti-counterfeiting materials.[36,37] Moreover, considering GO has favorable dispersibility in many solvents (water, ethylene glycol, N-methyl pyrrolidone, N, N-dimethyl formamide and etc.)[38], the realization of widely dispersibility, feature simplicity in process and GO LCs with different layers may have great potential applications in functional energy materials, such as flexible electrodes, electric circuits and chemical sensors, etc. [39-42]

## Acknowledgements

We are grateful to the National Natural Science Foundation of China (No. 51173170, 21101141), the financial support from the Innovation Talents Award of Henan Province (114200510019), State Key Laboratory of Chemical Engineering (No. SKL-ChE-13A04), and the Key program of science and technology (121PZDGG213) from Zhengzhou Bureau of science and technology.

## Notes and references

1 S. H. Aboutalebi, M. M. Gudarzi, Q. B. Zheng and J. K. Kim, *Adv. Funct. Mater.*, 2011, **21**, 2978.
2 Z. Xu, Y. Zhang, P. G. Li and C. Gao, *ACS Nano*, 2012, **6**, 7103.
3 R. R. Wang, J. Sun, L. A. Gao, C. H. Xu, J. Zhang and Y. Q. Liu, *Nanoscale*, 2011, **3**, 904.
4 Z. Xu and C. Gao, *ACS Nano*, 2011, **5**, 2908.
5 Z. Xu and C. Gao, *Nat. Commun.*, 2011, **2**, 571.
6 J. E. Kim, T. H. Han, S. H. Lee, J. Y. Kim, C. W. Ahn, J. M. Yun and S. O. Kim, *Angew. Chem., Int. Ed.*, 2011, **50**, 3043.
7 S. Zhang, I. A. Kinloch and A. H. Windle, *Nano Let.*, 2006, **6**, 568.
8 N. Behabtu, J. R. Lomeda, M. J. Green, A. L. Higginbotham, A. Sinitskii, D. V. Kosynkin, D. Tsentalovich, A. Nicholas, G. Parra-Vasquez, J. Schmidt, E. Kesselmann, Y. Cohen, Y. Talmon, J. M. Tour and M. Pasquali, *Nat. Nanotechnol.*, 2010, **5**, 406.
9 L. P. Tong, W. Qi, M. F. Wang, R. L. Huang, R. X. Su and Z. M. He, *Chem. commun.*, 2014, **50**, 7776.
10 X. M. Sun, Z. Liu, K. Welsher, J. T. Robinson, A. Goodwin, S. Zaric, and H. J. Dai, *Nano Res.*, 2008, **1**, 203.
11 X. M. Sun, D. C. Luo, J. F. Liu and D. G. Evans, *ACS Nano*, 2010, **4**, 3381.

12 X. l. Wang, H. Bai, and G. Q. Shi, *J. Am. Chem. Soc.*, 2011, **133**, 6338.
13 W. S. Hummers and R. E. Offeman, *J. Am. Chem. Soc.*, 1958, **80**, 1339.
14 V. C. Tung, M. J. Allen, Y. Yang and R. B. Kaner, *Nat. Nanotechnol.*, 2009, **4**, 25.
15 Y. Geng, S. J. Wang, J. K. Kim, *J. Colloid Interface Sci.* 2009, **336**, 592.
16 Y. Gao, W. C. Ren, T. Ma, Z, B. Liu, Y Zhang, W. B. Liu and L. P. Ma, ACS Nano, 2013, **7**, 5199.
17 J. P. Rourke, P. A. Pandey, J. J. Moore, M. Bates, I. A. Kinloch, R. J. Young and N. R. Wilson, Angew. Chem. Int. Ed., 2011, 50, 3173.
18 K. Krishnamoorthy, M. Veerapandian, K. Yun and S. J. Kim, *Carbon*, 2013, **53**, 38.
19 D. Li, M. B. Muller, S. Gilje, R. B. Kaner and G. G. Wallace, *Nat. Nanotechnol.*, 2008, **3**, 101.
20 J. Chen, B. W. Yao, C. Li, G. Q. Shi. *Carbon*, 2013, **64**, 225.
21 D. C. Marcano, D. V. Kosynkin, J. M. Berlin, A. Sinitskii, Z. Z. Sun, A. Slesarev, L. B. Alemany, W. Lu and J. M. Tour. *ACS Nano*, 2010, **4**, 4806.
22 L. Onsager, Ann. N. Y, *Acad. Sci.*, 1949, **51**, 627.
23 F. Guo, F. Kim, T. H. Han, V. B. Shenoy, J. X. Huang and R. H. Hurt, *ACS Nano*, 2011, **5**, 8019.
24 C. Zamora-Ledezma, N. Puech, C. Zakri, E. Grelet, S. E. Moulton, G. G. Wallace, S. Gambhir, C. Blanc, E. Anglaret and P. Poulin, *Journal of Physical Chemistry Letters,* 2012, **3**, 2425.
25 Y. Zhu, S. Murali, W. Cai, X. Li, J. W. Suk, J. R. Potts and R. S. Ruoff, *Adv. Mater.*, 2010, **22**, 3906.
26 X. Huang, X. Qi, F. Boey and H. Zhang, Graphene-based composites, *Chem. Soc. Rev.*, 2012, **41**, 666.
27 S. F. Pei and H. M. Cheng, *Carbon*, 2012, **50**, 3210.
28 J. Zhao, S. Pei, W. Ren, L. Gao and H. M. Cheng, *Acs Nano*, 2010, **4**, 5245.
29 S. F. Pei, J. P. Zhao, J. H. Du, W. C. Ren and H. M. Cheng, *Carbon*, 2010, **48**, 4466.
30 M. S. Dresselhaus, A. Jorio, M. Hofmann, G. Dresselhaus and R. Saito, *Nano Lett.*, 2010, **10**, 751.
31 O. C. Compton and S. T. Nguyen, *Small*, 2010, **6**, 711.
32 Y. Xu, K. Sheng, C. Li and G. Q. Shi, *ACS Nano*, 2010, **4**, 4324.
33 L. Estevez, A. Kelarakis, Q. Gong, E. H. Da'as and E. P. Giannelis, *J. Am. Chem. Soc.*, 2011, **133**, 6122.
34 M. A. Worsley, P. J. Pauzauskie, T. Y. Olson, J. Biener, J. H. Satcher Jr. and T. F. Baumann, *J. Am. Chem. Soc.*, 2010, **132**, 14067.
35 Z. P. Chen, W. C. Ren, L. B. Gao, B. L. Liu, S. F. Pei and H. M. Cheng, *Nat. Mater.*, 2011, **10**, 424.
36 Y. P. Zhang, V. P. Chodavarapu, A. G. Kirk and M. P. Andrews, *J. Nanophoton.*, 2012, **6**, 1.
37 M. P. De Santo, G. Petriashvili, R. Gary, G. Pucci and R. Barberi, *Rend. Lincei*, 2015, **26**, 255.
38 R. Jalili, S. H. Aboutalebi, D. Esrafilzadeh, K. Konstantinov, S. E. Moulton, J. M. Razal and G. G. Wallace, *ACS Nano*, 2013, **7**, 3981.
39 P. Blake, P. D. Brimicombe, R. R. Nair, T. J. Booth, D Jiang, F. Schedin, L. A. Ponomarenko, S. V. Morozov, H. F. Gleeson, E. W. Hill, A. K. Geim and K. S. Novoselov, *Nano lett.*,2008, 8, 1704.
40 C. Zhu, T. Y-J. Han, E. B. Duoss, A. M. Golobic, J. D. Kuntz, C. M. Spadaccini and M. A. Worsley, *Nat. Commun.*, 2015, **6**, 1.
41 S. Lawes, A. Riese, Q. Sun, N. Cheng and X. l. Sun, *Carbon*, 2015, **92**, 150.
42 X. j. Wei, D. Li, W. Jiang, Z. M. Gu, X. J. Wang, Z. X. Zhang and Z. Z. Sun, *Sci. Rep.*, 2015, **5**, 1.

# Liquid Crystal Graphene Oxide with different layers: Fabrication, Characterization and Applications

Jianmin Zhang, Yumei Ren, Tao Xu, Hongxia Yang and Qun Xu*

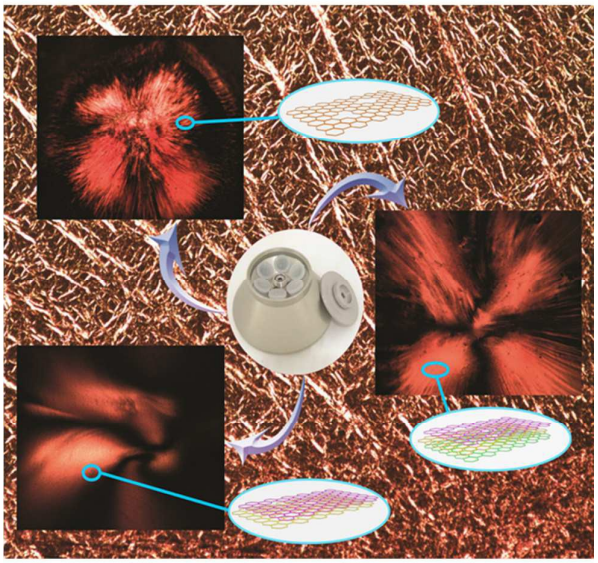

Graphene oxide liquid crystals with different layers were successfully prepared via simple centrifugation. The self-assemblied film demonstrates radial schlieren textures (the background) and has a high electrical conductivity.